Journal of Oceanography, Vol. 64, pp. 1 to 21, 2008

South China Sea Wave Characteristics during Typhoon Muifa Passage in Winter 2004

PETER C. CHU* and KUO-FENG CHENG

Naval Ocean Analysis and Prediction (NOAP) Laboratory, Department of Oceanography, Naval Postgraduate School, Monterey, CA 93943, U.S.A.

(Received 11 September 2006; in revised form 31 July 2007; accepted 10 August 2007)

The responses to tropical cyclones of ocean wave characteristics in deep water of the western Atlantic Ocean have been investigated extensively, but not the regional seas in the western Pacific such as the South China Sea (SCS), due to a lack of observational and modeling studies there. Since monsoon winds prevail in the SCS but not in the western Atlantic Ocean, the SCS is unique for investigating wave characteristics during a typhoon's passage in conjunction with steady monsoon wind forcing. To do so, the Wavewatch-III (WW3) is used to study the response of the SCS to Typhoon Muifa (2004), which passed over not only deep water but also the shallow shelf of the SCS. The WW3 model is forced by the NASA QuikSCAT winds and tropical cyclone wind profile model during Typhoon Muifa's passage from 0000UTC 16 on November to 1200UTC on 25 November 2004. The results reveal the unique features of the SCS wave characteristics in response to Muifa, such as non-decaying, monsoon-generated swell throughout the typhoon period and strong topographic effects on the directional wave spectrum.

Keywords:
- Directional wave spectrum,
- northeast monsoon,
- QuikSCAT winds,
- significant wave height,
- South China Sea,
- TOPEX/ POSEIDON altimetry,
- typhoon,
- Wavewatch-III.

1. Introduction

A moving tropical cyclone is an intense source of surface wind stress that causes many significant changes in the ocean wave characteristics, such as significant wave height, directional wave spectra, and wave propagation. These features have been well identified in open oceans such as the western Atlantic without monsoon winds (e.g., Moon *et al*., 2003). A hurricane, with intense rapidly varying winds, produces a severe, complex ocean wave field that can propagate for thousands of kilometers away from the storm center, resulting in dramatic variation of the wave field in space and time (Barber and Ursell, 1948). To investigate the wave characteristics, the directional spectra of hurricane-generated waves were measured using variety of instruments. For example, the fetch effect was detected in the Celtic Sea using high-frequency radar (Holden and Wyatt, 1992). The wave characteristics were obtained for the northeast Pacific during passage of the storm using the synthetic aperture radar image from the ERS-1 satellite (Holt *et al*., 1998). The spatial wave variations of hurricane directional wave spectra were identified for both open ocean and landfall cases using the NASA scanning radar altimeter (Walsh *et al*., 1989; Wright *et al*., 2001). Hwang and Wang (2001) computed the directional wave spectra from the ocean surface fluctuation.

The ocean wave response identified in open oceans without monsoon winds is a significant right-forward-quadrant bias in the significant wave height. During the passage of Hurricane Bonnie (1998) in the Atlantic Ocean, both observational (Wright *et al*., 2001) and modeling (Moon *et al*., 2003) studies show that the significant wave height reaches 14 m. The maximum wave heights appear in the right forward quadrant of the hurricane center and propagate in the same direction as the hurricane. Moon *et al*. (2003) simulated the wave characteristics successfully using the wave model Wavewatch-III (hereafter referred to as WW3) and found that the hurricane-generated wave field is mostly determined by two factors: the distance from the hurricane center or radius of maximum winds (RMW, represented by $R_{\max}$) and hurricane translation speed. For the case of a hurricane with low translation speed, the dominant wave direction is mainly determined by the distance from the hurricane center.

However, wave characteristics have not been well identified in regional seas with complex topography and monsoon winds, such as the South China Sea (SCS). The SCS is a semi-enclosed tropical sea located between the

* Corresponding author. E-mail: pcchu@nps.edu

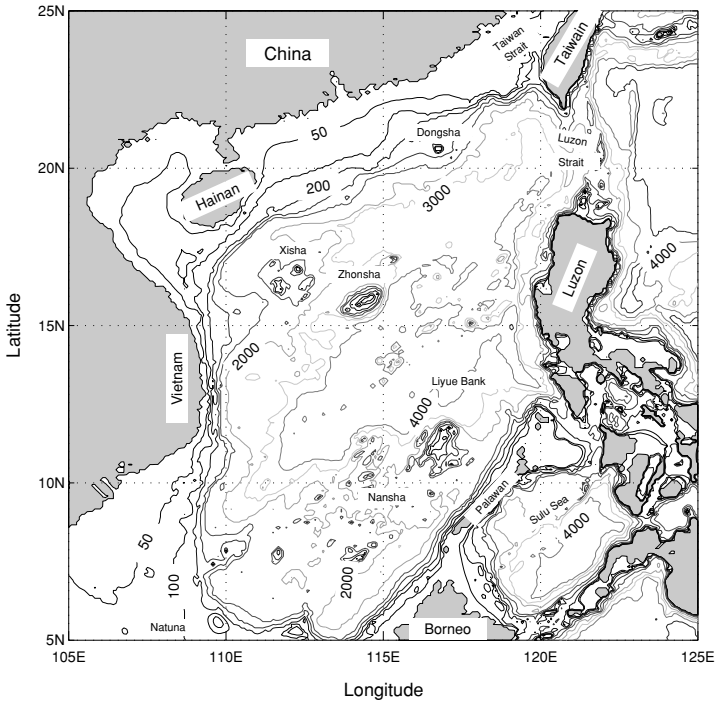

Fig. 1. Geography of the South China Sea.

Asian land mass to the north and west, the Philippine Islands to the east, Borneo to the southeast, and Indonesia to the south (Fig. 1), covering a total area of 3.5×10^6 km^2. It includes the shallow Gulf of Thailand and connections to the East China Sea (through the Taiwan Strait), the Pacific Ocean (through the Luzon Strait), the Sulu Sea, the Java Sea (through the Gasper and Karimata Straits) and the Indian Ocean (through the Strait of Malacca). All of these straits are shallow except the Luzon Strait, the maximum depth of which is 1800 m. The complex topography includes the broad shallows of the Sunda Shelf in the south/southwest; the continental shelf of the Asian landmass in the north, extending from the Gulf of Tonkin to the Taiwan Strait; a deep, elliptically shaped basin in the center; and numerous reef islands and underwater plateaus scattered throughout. The shelf, which extends from the Gulf of Tonkin to the Taiwan Strait, is consistently nearly 70 m deep and averages 150 km in width; the central deep basin is 1900 km along its major axis (northeast-southwest) and approximately 1100 km along its minor axis, and extends to over 4000 m deep. The Sunda Shelf is the submerged connection between southeastern Asia, Malaysia, Sumatra, Java, and Borneo and reaches 100 m depth in the middle; the center of the Gulf of Thailand is about 70 m deep. Furthermore, the SCS is subjected to a seasonal monsoon system (Chu *et al*., 1999, 2000a, 2000b). From April to August, the weaker southwesterly summer monsoon winds result in a wind stress about 0.1 N m^{-2}. From November to March, the stronger northeasterly winter monsoon winds correspond to a maximum wind stress of 0.3 N m^{-2}. The transition periods are marked by highly variable winds and surface currents. Thus, the SCS is a perfect location for studying wave characteristics in regional seas with complex topography and monsoon winds. Another benefit of doing so is that the WW3 has been implemented and verified for the SCS using TOPEX/POSEIDON (T/P) satellite data (Chu *et al*., 2004).

The major goal of this paper is to detect the unique feature of wave conditions during typhoon passage in the SCS because of the unique topographical configuration and the existence of monsoon winds. More specifically, we study the SCS responses to Typhoon (TY) Muifa (2004) using WW3. The outline of the paper is as follows. Section 2 describes movement of TY Muifa 2004 over the SCS. Section 3 delineates the establishment of the wind data using the NASA QuikSCAT Level 3 data and the tropical cyclone wind profile model (TCWPM). Section 4 depicts the WW3 model. Section 5 describes the wave characteristics including significant wave height and directional wave spectra. Section 6 shows the effects of typhoon translation speed, intensity, monsoon winds, and topography on the wave characteristics, and Section 7 gives the conclusions.

2. Typhoon Muifa 2004

TY Muifa is one of the four tropical cyclones to pass by the SCS in 2004. It was formed on 14 November (according to the best track data) and weakened over land on 26 November. The track passage of TY Muifa (Fig. 2) and record (Table 1) were provided by the Joint Typhoon Warning Center (JTWC, 2005). The translation speed of TY Muifa is calculated from the distance between typhoon center positions reported by JTWC.

2.1 Formation over the western Pacific

TY Muifa was first generated as a tropical depression on 14 November 2004 in the Western North Pacific Ocean. It moved westward at first and turned northwestward, passing north of Palau before entering the Philippine Sea. The disturbance was first mentioned by JTWC at 1600UTC 13 November, approximately 400 km north of Palau. The depression was developed into a tropical storm at 1400UTC on 14 November. According to its strength, the Japan Meteorological Agency first named it Muifa. However, the Philippine Atmospheric, Geophysical, and Astronomical Services Administration assigned the name Unding at 0000UTC 14 November, after the tropical cyclone had invaded their area of responsibility.

Muifa was steadily upgraded as it moved west-northwestward to the Philippines. It began the clockwise loop at 1200UTC 17 November and continued for several days. On 18 November, the intensity of TY Muifa reached the maximum wind speed at 59.2 m/s at 1200UTC, and then a remarkable weakening phase began.

2.2 Entering the SCS

TY Muifa was weakened to 54 m/s at 0000UTC 19 November and slowly headed towards the southwest. It moved slowly south-southwestward across Luzon and entered the SCS. Its intensity was further weakened to 30.9 m/s and downgraded to a tropical storm (TS) at 1200UTC 20 November.

At 0000UTC 21 November, TS Muifa was re-intensified to 33.4 m/s and upgraded back to a typhoon. Further strengthening occurred as TY Muifa went west-southwestwards across the warm waters of the SCS. The intensity of TY Muifa reached the second peak of 46.3 m/s at 1800UTC at (11.6°N, 114.4°E), approximately 800 km east of Vietnam. TY Muifa continued its journey to Vietnam from 22 to 23 November and was weakened again. The maximum wind speed was further decreased to 23.2 m/s at 1200UTC 24 November.

2.3 Weakening

Muifa was weakened to 15.4 m/s and downgraded to tropical depression status at 1200UTC 25 November. At 0000UTC 26 November Muifa turned northward into an environment of increased wind shear and as the intensity had fallen to 12.9 m/s, JTWC issued the final warning on TC Muifa. The final position was 250 km south-southwest of Bangkok, Thailand.

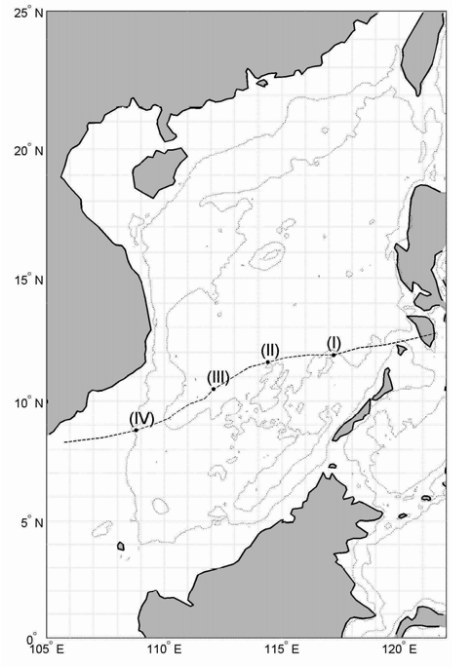

Fig. 2. Track of TY Muifa during 16–25 November 2004. Here, the numbers indicate the dates of the month and solid dots denote 0000 GMT of the corresponding dates: (I) November 21, (II) November 22, (III) November 23, and (IV) November 24. Dotted lines indicate the water depths of 100 m (near shore) and 2000 m (deep water).

2.4 Typical locations along the typhoon track

The translation velocity, low pressure, intensity, and bathymetry vary along the track of the TY Muifa passage (Fig. 3). Four locations along the TY passage have been selected (Fig. 2) to investigate the effect of bottom topography and intensity and translation speed of TY Muifa on the wave characteristics: L-I (arriving SCS), L-II (strengthening and slowing), L-III (weakening), and L-IV (shelf breaking).

The TY Muifa center was located at L-I (11.9°N, 117.2°E) at 0000UTC on November 21 just after it entered the SCS 24 hr earlier. The typhoon translation speed slightly decreased to 5.8 m/s. The typhoon low pressure was 976 hPa with a maximum wind speed of 33.4 m/s. The estimated RMW is 24.4 km.

The TY Muifa center was located at L-II (11.6°N, 114.4°E) at 1800UTC on 21 November when it reached the strongest intensity (i.e., the lowest center pressure, 954 hPa). The maximum wind speed was 46.3 m/s, and

Table 1. Best track record and estimated radius parameters (R_S, R_{max}, R_0) of TY Muifa (2004) during 0000UTC 16 November to 0600UTC 25 November 2004 (from JTWC, 2005). Here (R_{18}, R_{26}, R_{33}) are the radii of wind speed of (18, 36, 33) m/s, and R_{max} the radius of maximum wind speed.

Date	Time	Lat. (°N)	Lon. (°E)	Type	TS (m/s)	P (μPa)	V_{max} (m/s)	R_{18} (km)	R_{26} (km)	R_{33} (km)	R_s (km)	R_{max} (km)	R_0 (km)
11/16/2004	00:00	14.5	125.7	TS		994	20.6	148	—	—	54.8	89.3	630
11/16/2004	06:00	14.5	124.9	TS	3.99	991	23.1	183	—	—	54.2	88.9	680
11/16/2004	12:00	14.5	124.2	TS	3.99	984	28.3	183	56	—	43.2	71.8	678
11/16/2004	18:00	14.4	123.6	TS	3.49	984	28.3	174	56	—	32.6	54.8	666
11/17/2004	00:00	14.6	123.6	TS	3.04	980	30.9	219	70	—	36.6	61.5	725
11/17/2004	06:00	14.8	123.6	TY	1.03	976	33.4	213	74	28	18.9	32.2	623
11/17/2004	12:00	15.2	123.8	TY	1.03	967	38.6	213	74	28	23.8	40.5	725
11/17/2004	18:00	15.5	123.8	TY	2.29	954	46.3	174	74	46	10.4	17.9	638
11/18/2004	00:00	15.7	123.8	TY	1.54	938	54	156	65	46	8.1	14.0	655
11/18/2004	06:00	15.9	123.9	TY	1.03	927	59.2	167	65	46	8.1	14.0	693
11/18/2004	12:00	15.9	124.2	TY	1.14	927	59.2	170	70	46	8.1	14.0	693
11/18/2004	18:00	15.7	124.4	TY	1.49	938	54	133	59	41	8.1	14.0	655
11/19/2004	00:00	15.2	124.2	TY	1.43	938	54	109	59	41	8.1	14.0	670
11/19/2004	06:00	14.7	124.1	TY	2.76	954	46.3	139	59	41	8.1	14.0	615
11/19/2004	12:00	14.2	123.7	TY	2.62	958	43.7	144	59	41	9.3	16.0	631
11/19/2004	18:00	13.7	122.8	TY	3.26	963	41.2	131	56	37	9.8	16.9	629
11/20/2004	00:00	12.8	121.6	TY	5.18	967	38.6	137	56	37	10.6	18.2	661
11/20/2004	06:00	12.5	120.3	TY	7.59	976	33.4	137	56	—	15.7	26.9	663
11/20/2004	12:00	12.3	119.3	TS	6.71	980	30.9	115	56	—	16.8	28.7	646
11/20/2004	18:00	12.2	118.3	TY	5.13	976	33.4	115	56	—	13.7	23.5	648
11/21/2004	00:00	11.9	117.2	TY	5.06	976	33.4	128	56	—	14.2	24.4	667
11/21/2004	06:00	11.9	116.1	TY	5.75	972	36	152	56	28	14.7	25.2	710
11/21/2004	12:00	11.8	115.2	TY	5.54	963	41.2	152	65	37	10.6	18.3	714
11/21/2004	18:00	11.6	114.4	TY	4.56	954	46.3	152	65	37	8.1	14.0	725
11/22/2004	00:00	11.4	113.6	TY	4.16	958	43.7	152	65	37	9.1	15.7	729
11/22/2004	06:00	11.1	113.1	TY	4.16	958	43.7	126	59	33	8.1	14.0	718
11/22/2004	12:00	10.8	112.6	TY	2.96	967	38.6	120	52	33	10.4	17.9	721
11/22/2004	18:00	10.5	112.1	TY	2.96	976	33.4	120	52	33	16.7	28.6	763
11/23/2004	00:00	10.1	111.7	TY	2.96	976	33.4	120	52	—	12.8	22.0	726
11/23/2004	06:00	9.9	111.1	TY	2.89	976	33.4	111	56	—	11.7	20.1	716
11/23/2004	12:00	9.6	110.6	TS	3.21	980	30.9	109	48	—	14.3	24.6	733
11/23/2004	18:00	9.3	110.2	TS	2.97	984	28.3	107	44	—	16.7	28.6	738
11/24/2004	00:00	9.1	109.7	TS	2.55	984	28.3	107	44	—	16.7	28.6	749
11/24/2004	06:00	8.8	108.8	TS	2.74	987	25.7	120	52	—	23.7	40.4	795
11/24/2004	12:00	8.5	107.4	TS	4.83	994	20.6	102	—	—	33.7	56.9	775
11/24/2004	18:00	8.3	105.7	TS	7.29	994	20.6	93	—	—	30.4	51.5	763
11/25/2004	00:00	8.7	103.6	TS	8.72	994	20.6	93	—	—	30.5	51.6	739
11/25/2004	06:00	8.7	101.7	TS	10.9	997	18	96	—	—	47.3	78.8	772

RMW was 14.0 km. The typhoon translation speed slowed down to 4.2 m/s.

The TY Muifa center was located at L-III (10.5°N, 112.1°E) at 0000UTC on 23 November when it had the same intensity as at L-I. The translation speed is notably slower at L-III (2.9 m/s) than at L-I (5.8 m/s). The radius of maximum wind is slightly larger at L-III (RMW = 28.6 km) than at L-I (RMW = 24.4 km). Other conditions are the same at L-III (minimum pressure: 976 hPa, maximum wind speed: 33.4 m/s) as at L-I. L-III represents the typhoon weakening period. Comparison of wave characteristics between L-I and L-III shows the effect of the translation speed.

The TY Muifa center was located at L-IV (8.8°N,

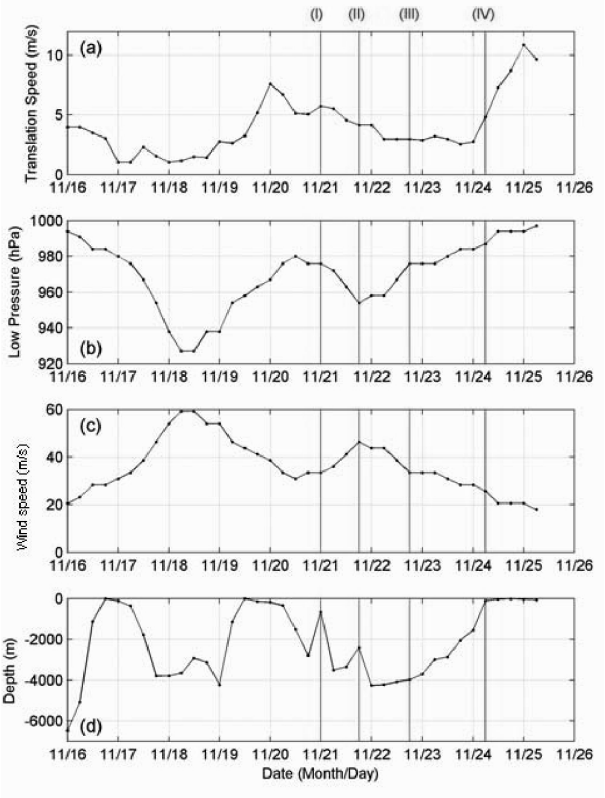

Fig. 3. Several parameters along the passage of TY Muifa (2004): (a) translation speed, (b) lowest pressure, (c) maximum wind speed, and (d) the water depth. Four lines indicate designated locations of typhoon centers.

108.8°E) at 0600UTC on 24 November where TY Muifa (8.8°N, 108.8°E) was close to the Asian landmass. At this time, the translation speed increases to 4.8 m/s. The water depth is about 116 m. The low pressure is 987 hPa, the maximum wind speed was 25.7 m/s with RMW of 40.4 km. The typhoon intensity is much weaker at L-IV than at L-II.

3. Typhoon Winds

In-situ measurements are difficult to conduct during the typhoon seasons. Remotely sensed data are generally used. The NASA QuikSCAT Level 3 data (0.25° × 0.25° resolution) were downloaded during the period of TY Muifa (2004). The evolution of QuikSCAT wind fields from 17 November to 25 November (Fig. 4) clearly shows that the typhoon strength agrees closely with the progress of TY Muifa into the SCS, but the structure of tropical cyclone winds is not well presented due to both the temporal limitation of a satellite pass and the inaccuracy of scatterometer data at high wind speeds.

Due to the spatial coverage, the strong rotational motion from TY Muifa may not be represented in the QuikSCAT data (Fig. 4). To overcome this deficiency, a Tropical Cyclone Wind Profile Model (TCWPM) (Carr and Elsberry, 1997) was used to produce the high resolution gridded surface wind field for TY Muifa.

3.1 Tropical cyclone wind profile model

A tropical cyclone wind profile model (TCWPM) (Carr and Elsberry, 1997) was used to establish a high-resolution surface wind field for TY Muifa 2004. Let (R_S, R_0) be the radius of scale, and radius of zero tangential velocity inside a tropical cyclone. Based on the angular momentum balance, Carr and Elsberry (1997) proposed a model to compute the wind vector relative to the center of the tropical cyclone,

$$v_c(r) = \frac{f_0}{2}\left[R_0\left(\frac{R_0}{r}\right)^X - r\right]\frac{a^4}{1+a^4}, \quad u_c(r) = \tan(\gamma)v_c(r), \tag{1}$$

where r is the horizontal distance to the storm center; (u_c, v_c) are the radial and tangential velocity components; $\gamma$is the inflow angle of the wind as it spirals into the center of the cyclone; a is a scaling factor ($a = r/R_S$) that makes $v_c(r)$ continuous at the center of the tropical cyclone. The inflow angle (γ) is defined as the angle between the typhoon wind vector (relative to the center) and the tangential direction. This angle is caused by the surface friction and is determined from surface weather maps or satellite images. X is a positive constant less than 1. Considering the beta effect propagation, Carr and Elsberry (1997) proposed a value of $X = 0.4$.

To prevent a large discontinuity at the periphery of the storm, however, the environmental wind field ($\mathbf{V}_{en}$) is blended into the tropical storm wind field. Let $\mathbf{V}_c = (v_c, u_c)$ be the wind vector relative to the TY center and $\mathbf{V}_t$ be the translation velocity. Adjustments were made near the storm's periphery to smooth the transition between the background and storm wind fields. This was done by taking a weighted average inside and outside of the tropical cyclone,

$$\mathbf{V} = (1-\varepsilon)(\mathbf{V}_c + \mathbf{V}_t) + \varepsilon\mathbf{V}_{en}, \tag{2}$$

where ε is the weight

$$\varepsilon = \frac{c^4}{1+c^4}, \quad c = \frac{r}{0.9R_0}. \tag{3}$$

The effects of these adjustments are to gradually increase the weighting on the storm wind and decrease the weighting on the environmental winds as the radial distance to

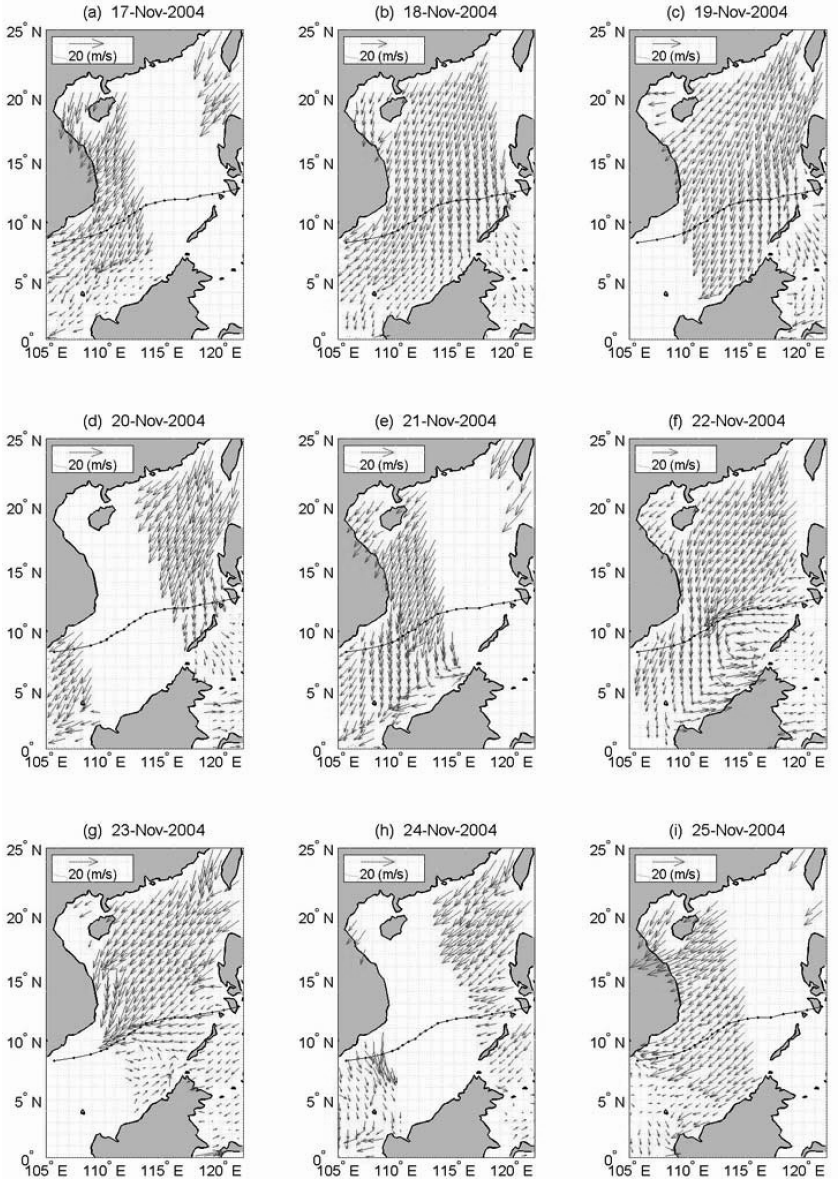

Fig. 4. Daily QuikSCAT wind vector fields on 17–25 November 2004.

the storm center decreases. Both effects provide for a smoother transition between the storm wind field and the environmental wind field.

3.2 Determination of model parameters

In TCWPM, as described in (1), the tangential wind depends on (r, R_S, R_0). Carr and Elsberry (1997) determine R_0 from the satellite image according to the size of overall convective and outflow cloud pattern of the TC. On the other hand, Chu *et al*. (2000b) fixed the values of radii for the entire typhoon passage. Since there is no satellite image available during TY Muifa passage in the SCS, the values of radii of TY Muifa are determined using the data from Table 1. Near the typhoon center, the winds reported by JTWC can be approximately taken as the tangential winds. Let tangential winds at (r_1, r_2, ..., r_k) be (v_1, v_2, ..., v_k). Equation (1) gives a set of nonlinear algebraic equations

$$\begin{aligned} v(r_1, R_0, R_S) &= v_1, \\ v(r_2, R_0, R_S) &= v_2, \\ &\vdots \\ v(r_k, R_0, R_S) &= v_k, \end{aligned} \tag{4}$$

where $(r_1, r_2, ..., r_k)$ and $(v_1, v_2, ..., v_k)$ are given. Since Eq. (4) is a set of nonlinear algebraic equations, there are usually no analytical solutions for (R_S, R_0). An iteration scheme is used to determine the values of (R_S, R_0). This scheme starts with a set of first-guess values of $(R_S^{(0)}, R_0^{(0)})$. In this study we choose

$$R_S^{(0)} = 20 \text{ km}, \quad R_0^{(0)} = 1000 \text{ km}.$$

Substituting these values into (1), we obtain 0-th order calculated tangential winds $(v_1^{(0)}, v_2^{(0)}, ..., v_k^{(0)})$. The root-mean-square (RMS) error for mismatch between $(v_1, v_2, ..., v_k)$ and $(v_1^{(0)}, v_2^{(0)}, ..., v_k^{(0)})$ is computed by

$$\text{RMS}^{(n)} = \sqrt{\frac{1}{k}\sum_{j=1}^{k}\left(v_j^{(n)} - v_j\right)^2},$$

where $n = 0$. We expect $\text{RMS}^{(0)}$ to be large.

Second, we use the iteration method to obtain optimal (R_S, R_0) with an incremental adjustment ($\Delta R_S = 0.1$ km, $\Delta R_0 = 1$ km) at each step. From the n-th order (n starting from 0, the first-guess) set, $(R_S^{(0)}, R_0^{(0)})$, we have eight (3^2–1) different combinations of the adjustment,

$$\left(R_S^{(n)} + \Delta R_S, R_0^{(n)}\right), \quad \left(R_S^{(n)} - \Delta R_S, R_0^{(n)}\right),$$
$$\left(R_S^{(n)}, R_0^{(n)} + \Delta R_0\right), \quad \left(R_S^{(n)}, R_0^{(n)} - \Delta R_0\right),$$
$$\left(R_S^{(n)} + \Delta R_S, R_0^{(n)} - \Delta R_0\right), \quad \left(R_S^{(n)} + \Delta R_S, R_0^{(n)} + \Delta R_0\right),$$
$$\left(R_S^{(n)} - \Delta R_S, R_0^{(n)} - \Delta R_0\right), \quad \left(R_S^{(n)} - \Delta R_S, R_0^{(n)} + \Delta R_0\right),$$

among which we pick a set with minimum RMS error as the $(n + 1)$-th order set of $(R_S^{(n+1)}, R_0^{(n+1)})$. We repeat this procedure until the minimum RMS error is achieved. At each iteration, $\text{RMS}^{(n)}$ is compared to a user specified criterion E_c. If $\text{RMS}^{(n)} < E_c$, we terminate the iteration and obtain an optimal set of (R_S, R_0). If $\text{RMS}^{(n)} > E_c$, we continue the iteration. In this study, E_c is set to 2 m/s. The estimated temporally varying (R_S, R_0) values are shown in Table 1. For example, (R_S, R_0) are (23.7 km, 795 km) at 0600UTC 24 November.

3.3 Environmental winds

Usually the environmental wind vectors ($\mathbf{V}_{en}$) (in (2)) change with time on synoptic scales. In this paper we study the effect of the Typhoon's passage on the surface wave characteristics by comparison between two simulations, one using $\mathbf{V}_{en}$ and the other using $\mathbf{V}$. The difference between the two simulations shows the Typhoon effect, and therefore for simplicity the environmental wind vector term ($\mathbf{V}_{en}$) in (2) is taken as the temporally averaged QuikSCAT Level 3 winds from both ascending and descending passes during 16–25 November 2004 (Fig. 5). The winds blow from northeast to southwest with a spatial average of about 7.8 m/s. This represents the dominant winter monsoon during the period of TY Muifa's passage in the SCS.

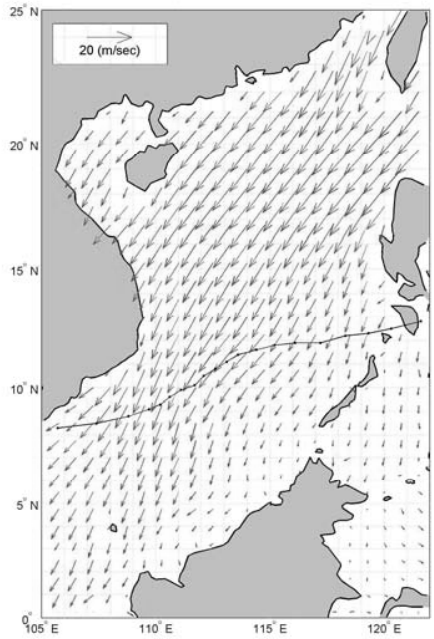

Fig. 5. Temporal mean QuikSCAT wind vector field from 0000UTC on 16 November to 0600UTC on 25 November 2004.

3.4 QuikSCAT-TCWPM winds

With the temporally mean QuikSCAT wind data as $\mathbf{V}_{en}$, the total wind field is computed from 0000UTC on 16 November to 0600UTC on 25 November for (0°–25°N, 105°E–122°E) using Eqs. (1) and (2) on a 1/4° × 1/4° grid with a time interval of 6 hr. Such a wind field is referred to as the QuikSCAT-TCWPM (QTCWPM) winds. The daily evolution of the QTCWPM winds (Fig. 6) shows that the wind speed increases as TY Muifa enters the SCS, and decreases as Muifa approaches the land. The QTCWPM maximum wind speed is comparable to the maximum wind speed reported in the best track record (46.3 m/s).

Surface winds greatly affect the wave characteristics. The QTCWPM winds (model-data combination) should be verified by observation. Unfortunately, there were no in-situ measurements of surface winds in the SCS during TY Muifa's passage. We compared the QTCWPM

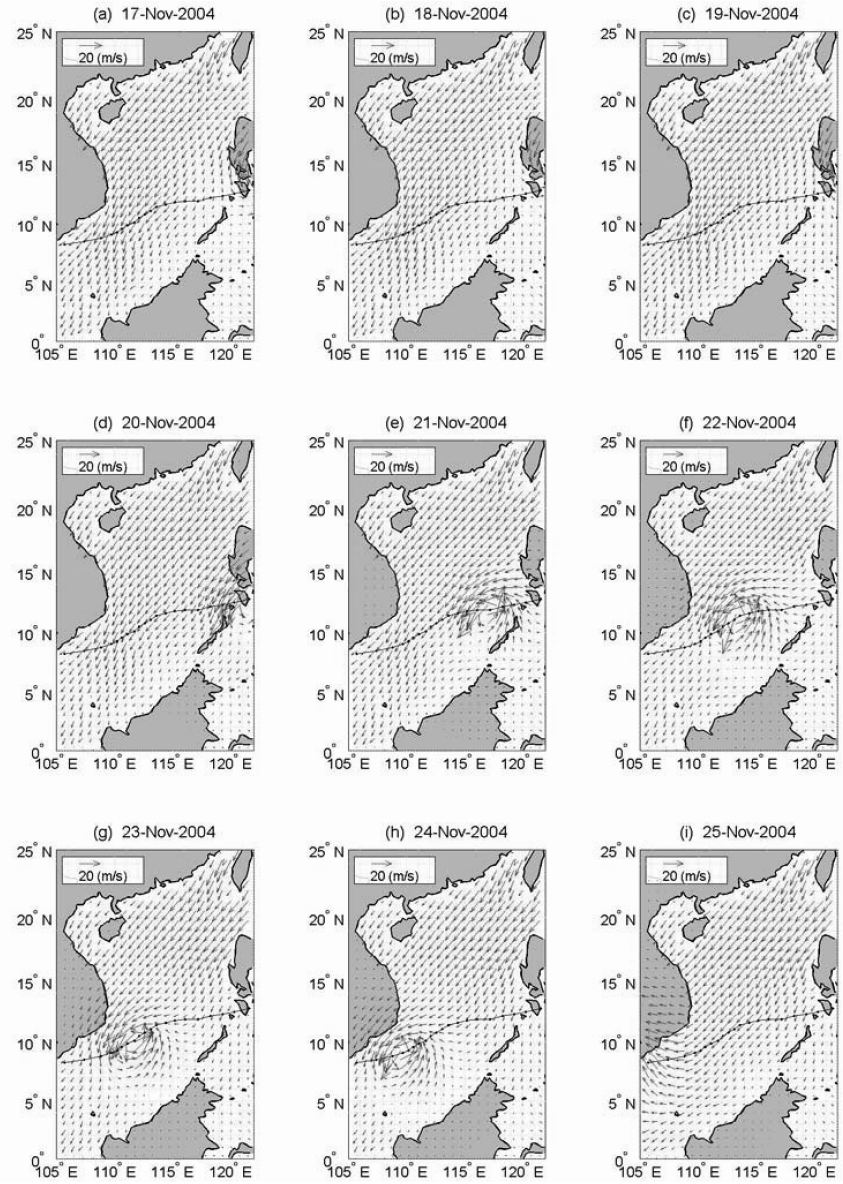

Fig. 6. Daily wind vector fields on 17–25 November 2004 from QTCWPM.

wind vectors (Fig. 6) to the QuikSCAT (Fig. 4) and the National Centers for Environmental Prediction (NCEP) surface wind vectors (Fig. 7). Obviously, TY Muifa was well represented by the QTCWPM winds thanks to the use of the JTWC data (Table 1), but not well represented by the QuikSCAT winds due to gaps in the satellite tracks, nor by the NCEP winds due to the deviation of TY Muifa from the typhoon track. To further evaluate the QTCWPM winds, we compute the RMS differences between the QTCWPM and QuikSCAT winds (3.2 m/s) and between the QTCWPM and NCEP winds (3.4 m/s). During TY Muifa's passage in the SCS, the averaged wind speed is around 35 m/s. Differences of this magnitude are not significant.

4. WW3 Model

4.1 Description

Spectral wave models usually predict the wave spectrum F, which is a function of phase parameters (i.e., wave number $\mathbf{k}$, direction θ, intrinsic frequency σ, and absolute frequency ω), space ($\mathbf{x}$), and time (t),

$$F = F(\mathbf{k}, \theta, \sigma, \omega; \mathbf{x}, t). \tag{5}$$

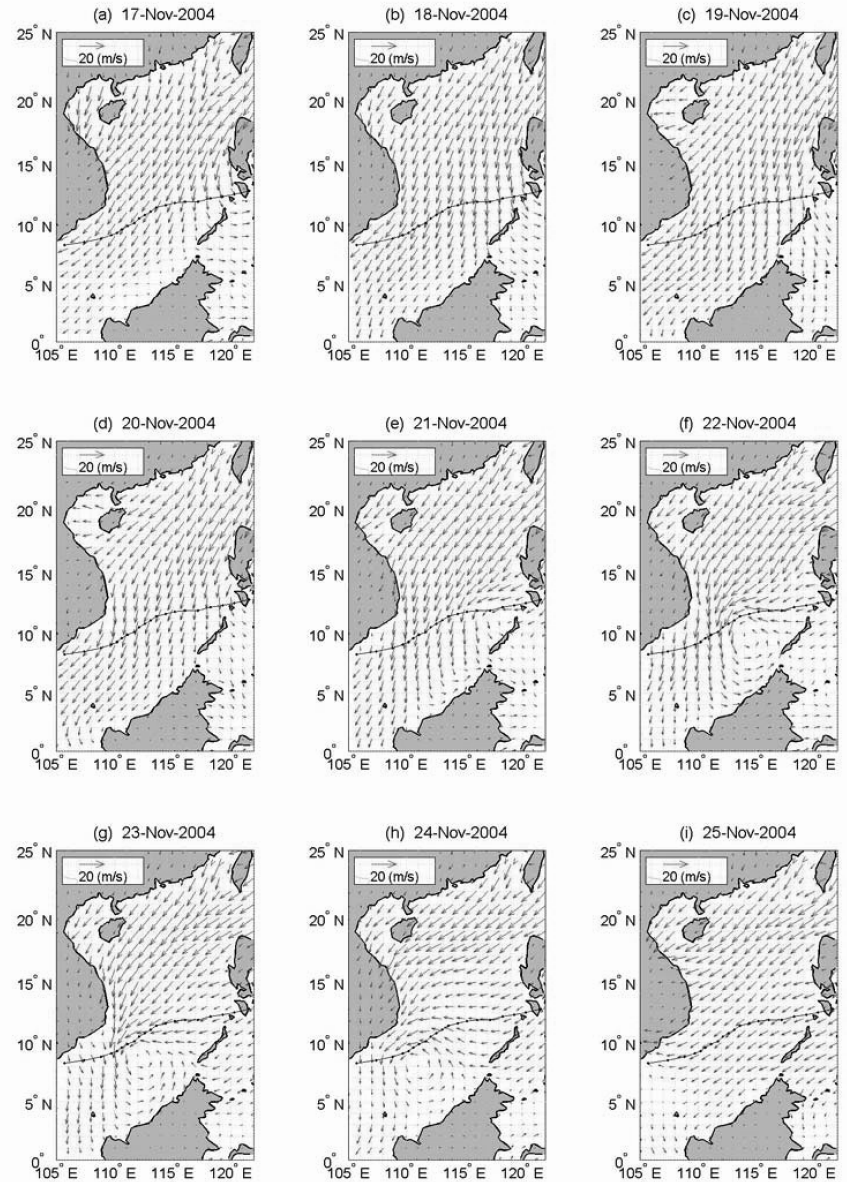

Fig. 7. Daily wind vector fields on 17–25 November 2004 from NCEP.

The linear wave theory (locally) gives the follow dispersion relation,

$$\sigma^2 = gk \tanh kd, \quad \omega = \sigma + \mathbf{k} \bullet \mathbf{U}, \tag{6}$$

where d is the mean water depth and $\mathbf{U}$ is the (depth- and time-averaged) current velocity. When the current velocity vanishes, only two phase parameters among (σ, $\mathbf{k}$, θ) are independent.

Without the ocean currents, the energy of a wave package is conserved. With the ocean currents the energy of a spectral component is no longer conserved (Longuet-Higgins and Stewart, 1961), but the wave action spectrum,

$$N(\mathbf{k},\theta,\mathbf{x},t) \equiv F(\mathbf{k},\theta,\mathbf{x},t)/\sigma,$$

is conserved (Whitham, 1965; Bretherthon and Garrett, 1968), and therefore WW3 uses the balance equation for the wave action spectrum (N) with the wavenumber-direction ($\mathbf{k}$, θ) as the independent phase variables (Tolman, 1999).

In this study, the ultimate quickest propagation scheme is selected with the dispersion correction taken

from Booij and Holthuijsen (1987); nonlinear interactions are included; and the source term parameterization follows Tolman and Chalikov (1996), Wittmann and Farra (1997), Tolman *et al*. (2002), and Chu and Cheng (2007), consisting of four parts: wind input, nonlinear wave-wave interaction, dissipation, and wave-bottom interaction. The output of WW3 consists of the traditional frequency-direction spectrum $F(\sigma, \theta)$, which is calculated from $F(\mathbf{k}, \theta)$ using Jacobean transformations.

4.2 Discretization

Following NCEP's operational wave prediction in the western North Atlantic Ocean during Hurricane Isabel (Tolman *et al*., 2005), a regularly spaced longitude-latitude grid with spacing 0.25° is used. This is also due to the comparable resolution (0.25°) in the QuikSCAT winds, which is much coarser in the JTWC data (see Table 1). For a moving hurricane with a translation speed of 7 m/s, the typhoon already moved 150 km after 6 hr. This horizontal resolution may be too coarse to resolve typhoon-generated wave fields since the minimum RMW can reach 14 km. With the enhancement of horizontal resolution in surface wind observation, higher resolution should be used in the wave simulation.

Four time steps are used in WW3 to achieve computational efficiency: (a) global time step (300 s) for the propagation of the entire solution, (b) spatial time step (300 s) representing the spatial propagation, (c) spectral time step (300 s) for intra-spectral propagation, and (d) source time step (100 s) for the source term integration.

The wavenumber grid spacing is determined by the frequency intervals (total 25)

$$\sigma_{m+1} = X_\sigma \sigma_m, \quad m = 0,1,\ldots,24, \tag{7}$$

with

$$X_\sigma = 1.1, \quad \sigma_0 = 0.0418. \tag{8}$$

The grid spacing of wave direction is 15° (i.e., $\Delta\theta = 15°$).

4.3 Model integration and verification

As a typhoon passes by, wind speed and direction changed rapidly. The typhoon-generated waves can propagate across the SCS further than 1000 km. Along the wave propagation direction, obstructions provided by coastline and small islands generate the wave shadow zones. This feature implies that the SCS, which is a semi-close marginal sea, can be considered as a wave system that is independent of nearby oceans, except for the energy transform through the Luzon Strait, the depth of which reaches 1800 m. The Sulu Sea, which separated by the Palawan Island, can be seen as a different wave system from the SCS. Thus, the model is implemented for SCS (0°–25°N, 105°–122°E) using realistic bathymetry data from the Naval Oceanographic Office DBDB5 database (5′ × 5′ resolution). The JONSWAP-type spectral parameterizations are used at the open boundaries.

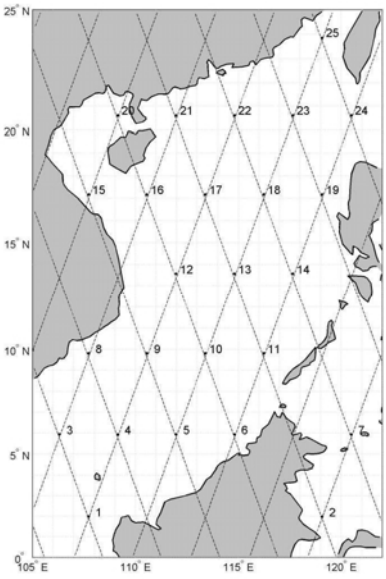

Fig. 8. TOPEX/Poseidon crossover points in the SCS.

Since TY Muifa was generated east of the SCS on 16 November, entered the SCS on 19 November 2004, and moved out of SCS on 25 November, we integrate the WW3-SCS from 0000UTC 16 November to 1200UTC 25 November (3 days earlier than the typhoon's entry time) with the QTCWPM winds $\mathbf{V}$ (Fig. 6), which is linearly interpolated into the source time step (100 s). The model output of the first three days (16–18 November) may not be realistic and will not be analyzed further. In modeling, the peak frequency (ω_p) is calculated by

$$\omega_p = 22\left(\frac{g^2}{VF}\right)^{1/3}, \tag{9}$$

where $V = |\mathbf{V}|$; g is the gravitational acceleration; and F is the fetch.

Due to lack of direct-measurement platforms, such as vessels or buoys, during typhoon seasons in the SCS, the T/P significant wave height (H_S) data are used for model verification. Fourteen passes across the SCS area (001, 012, 038, 051, 064, 077, 088, 114, 127, 140, 153, 164, 216, and 229) (from 11 November 2004 to 01 December) are available during the TY Muifa-2004 passage. These passes have a total of 25 crossover points (Fig. 8). Similar to Chu *et al*. (2004) and Tolman *et al*. (2005), the

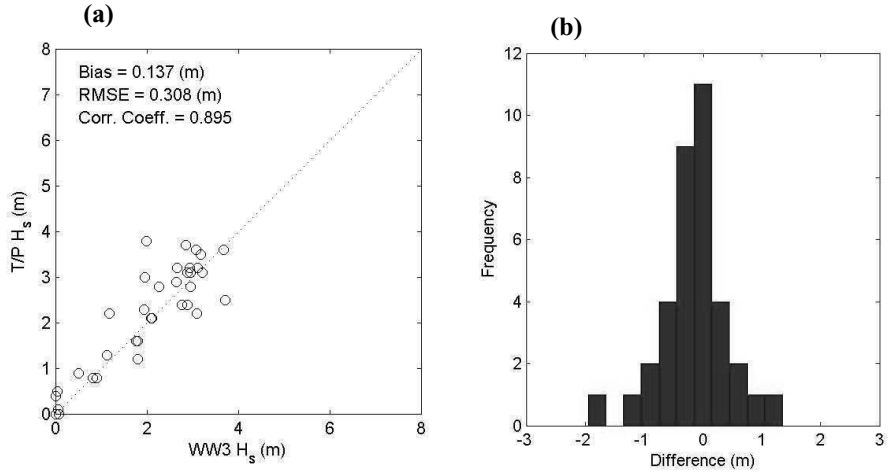

Fig. 9. Comparison of significant wave height between model (WW3) simulated and observed (TOPEX/POSEIDON) at all crossover points during the passage of TY Muifa (2004): (a) scatter diagram, and (b) histogram distribution of difference between modeled and observed values.

comparison was conducted along the passages and crossover points. The same wave (WW3) and wind (QTCWPM) models with QuikSCAT winds were used to simulate the wave characteristics during TY Muifa's passage from 0000UTC on 16 November to 0600UTC on 25 November 2004 (this study) and TY Rumbia from 0000UTC on 2 December to 0600UTC on 9 December 2000 (Chu *et al*., 2004). The two tropical storms (Muifa-2004 and Rumbia-2000) had very similar tracks. Since the model-generated H_S fields compared well to the satellite observed H_S fields along several T/P tracks (figure 14 in Chu *et al*., 2004), we only show the comparison on the 25 crossover points for illustration. Tolman *et al*. (2005) also demonstrated the capability of WW3 in simulating wave characteristics in the western North Atlantic Ocean with hurricane Isabel 2003.

Figure 9 shows the comparison of H_S between WW3 result and T/P observation with a total of 38 data pairs. The clustering of points is approximately located around the equal line. The histogram of the differences between model and observation shows a Gaussian-type distribution. Examining the statistics, the bias of the two datasets is 0.137 m with a root mean square error of 0.308 m and correlation coefficient 0.895. The statistics suggests that the numerical wave simulation using WW3 during the period of TY Muifa is reasonably good.

5. Wave Characteristics

5.1 Significant wave height

Figure 10 shows the daily evolution of H_S in the SCS during the passage of TY Muifa. Here, the upper panels represent the spin-up period (Figs. 10(a) and (b)) (the H_S field might not be realistic during the spin-up period) and the period before TY Muifa entered the SCS (Fig. 10(c)); the middle panels (Figs. 10(d)–(f)) represent the period during TY Muifa's passage through the SCS; and the lower panels (Figs. 10(g)–(i)) represent the period after TY moved out from the SCS. Compared to the evolution of QTCWPM wind field (Fig. 6), a close correlation is found between H_S and the typhoon winds. High H_S values with high wind speed and high waves appear to the right of the typhoon's passage. The maximum H_S (16 m) occurs as TY Muifa reaches its lowest pressure in the SCS on 21 November.

Comparing Figs. 10(e) and (f) with Fig. 10(c) shows the difference between monsoon-generated (or environmental wind-generated) and typhoon-generated waves. The monsoon-generated wave field is mainly determined by the fetch (compare Figs. 6(c) and 10(c)), while the typhoon-generated wave field is mostly determined by two factors: the distance from the typhoon center (or the radius of maximum wind) and typhoon translation speed (compare Figs. 6(e)–(h) and 10(e)–(h)). TY Muifa's translation speed is much slower than 10 m/s in the SCS (Fig. 3(a)). It is smaller than the group velocity of high waves. The dominant wave direction is mainly determined by the distance from the typhoon center and therefore the high center of significant wave height is near the typhoon center (compare Figs. 6(f)–(h) and 10(f)–(h)). As TY Muifa moved out of the SCS on November 24–25 (Figs. 6(h) and (i)), high H_S occurs west of Luzon (Figs. 10(h) and (i)). This is the swell generated by the (northeast) monsoon-winds.

During TY Muifa's passage from 17 to 25 November, the maximum values of the QTCWPM wind speed

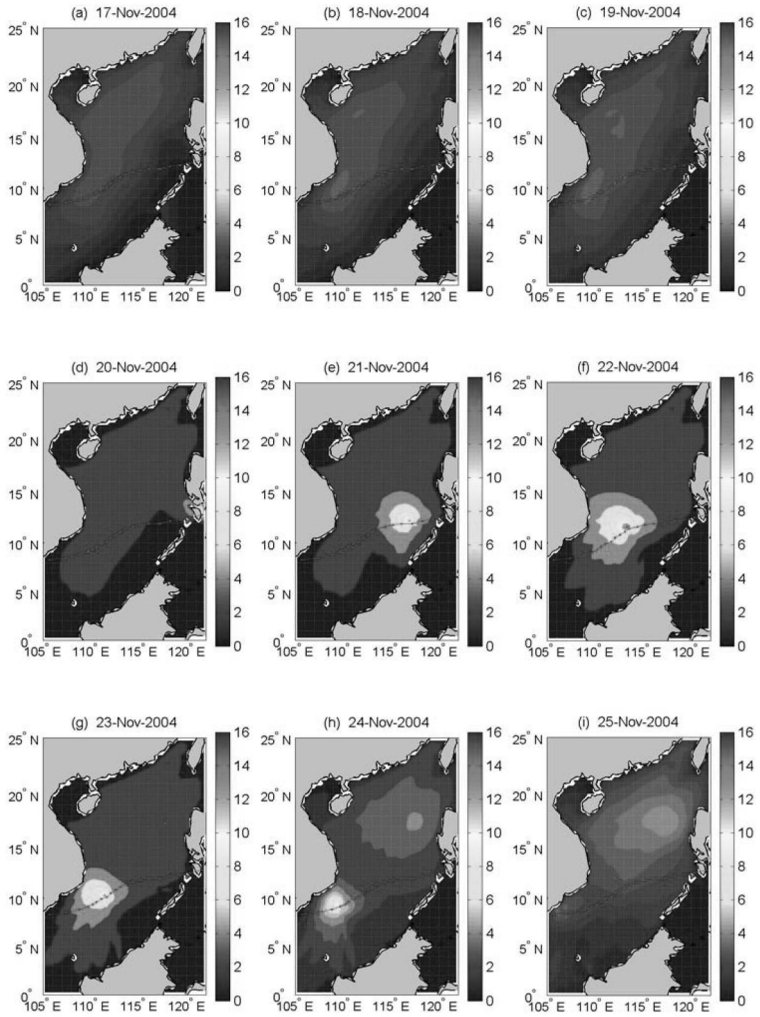

Fig. 10. Daily evolution of H_S in the SCS during the passage of TY Muifa (2004).

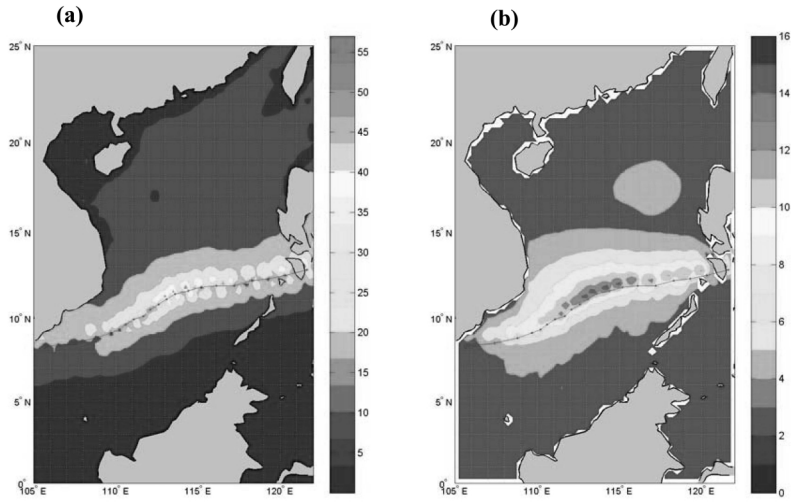

Fig. 11. Horizontal distributions during passage of TY Muifa (2004): (a) maximum QTCWPM wind speeds, and (b) maximum H_S calculated using WW3.

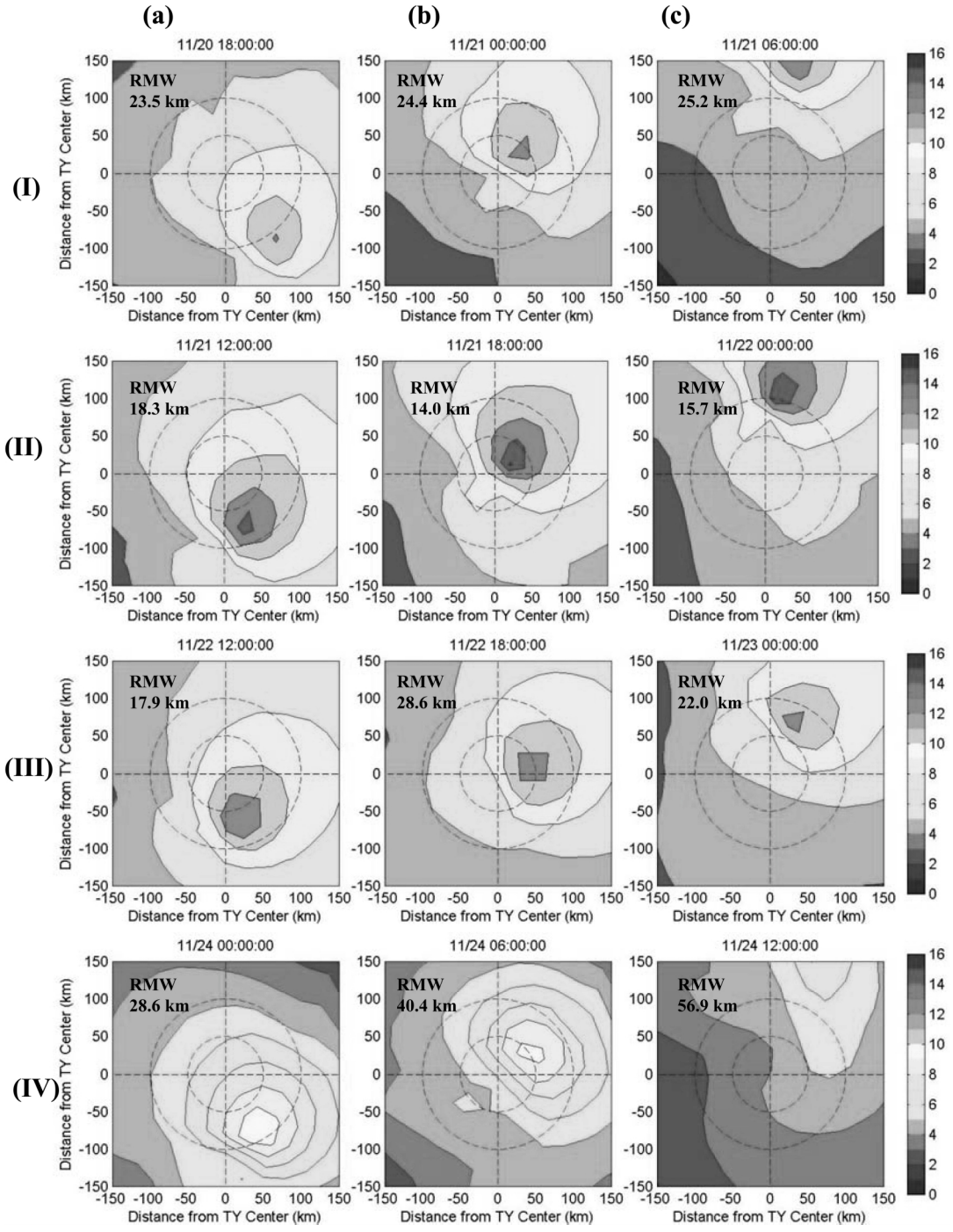

Fig. 12. Six-hour evolutions of H_S at four locations: (a) before typhoon's arrival (left column), (b) typhoon's right on (central column), and (c) after typhoon's departure (right column). Translation directions are rotated to the vertical axis.

and WW3 generated H_S are determined at each grid point (Fig. 11). The core of the maximum wind speed and H_S are asymmetric in width and in magnitude along the track of TY Muifa with higher wind speed and H_S on the right side of the track than the left side. Figure 12 shows 6-hr evolution of H_S at the typhoon center for all four locations (L-I to L-IV). The highest H_S is located outside RMW from the typhoon center in the right backward quadrant, six hours before the typhoon's arrival (Fig. 12(a)), in the right forward quadrant as the typhoon arrived (Fig.

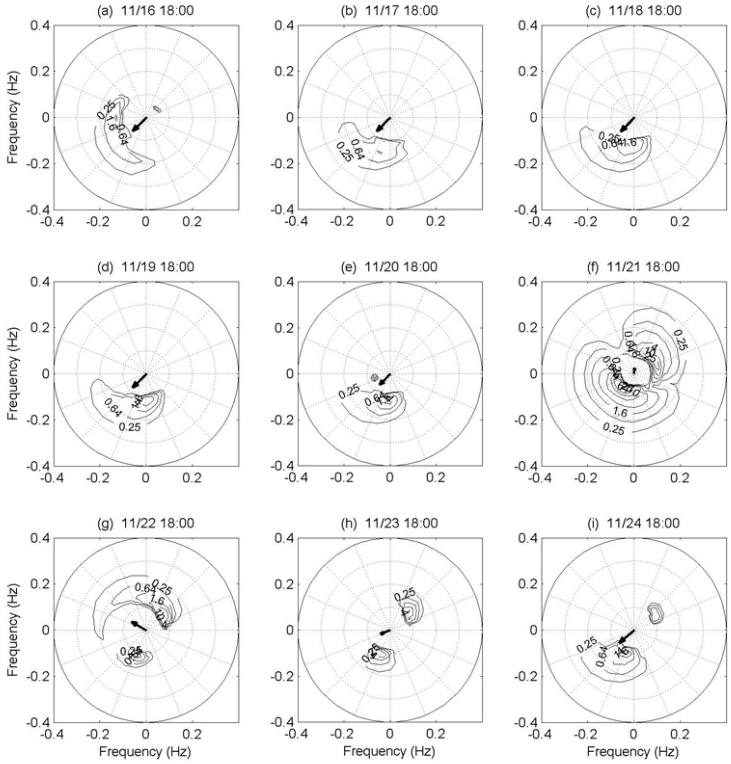

Fig. 13. Daily evolution of directional wave spectra with QTCWPM winds at L-II (11.6°N and 114.4°E). TY Muifa was at this location at 1800UTC on 21 November. Arrow presents QTCWPM wind speed and direction. Wind speed of 40 m/s corresponds to a length of 0.15 Hz.

12(b)) with a maximum H_S of 16 m, and in the right front quadrant (far away from the center) six hours after the typhoon's departure (Fig. 12(c)). The typhoon rapidly increases its translation speed after departure from the location L-IV (Fig. 3(a)), the highest H_S is furthest from the center among the four locations (Fig. 12(c)). Note that the calculated spectra contain the swell due to environmental winds (northeastern monsoon winds), and this makes the spectral shape complicated.

To investigate the effect of typhoon translation speed, the H_S fields have been rotated with the typhoon translation axis pointing upwards. L-I and L-III have comparable typhoon intensities (~33 m/s), water depths deeper than 600 m, but very different typhoon translation speeds (5.8 m/s at L-I and 2.9 m/s at L-III). Comparison of the H_S fields between L-I and L-III shows the effect of typhoon translation speed on H_S field. The maximum H_S is stronger and nearer to the typhoon center with lower translation speed (2.9 m/s at L-III) than with higher translation speed (5.8 m/s at L-I). L-II and L-IV have comparable typhoon translation speeds (4.2 and 4.8 m/s), but very different typhoon intensities. Comparison between L-II and L-IV shows the effect of the typhoon intensity on H_S field. The typhoon intensity does not change the spatial pattern of H_S field but reduces the maximum H_S from 16 m with intensity 46 m/s at L-II to 10 m with intensity 26 m/s at L-IV.

TY Muifa reached its highest intensity at L-II (11.6°N, 114.4°E) at 1800UTC on 21 November. Figure 12(b) shows the horizontal distribution of H_S at L-II with the typhoon translation axis being rotated towards the top and RMW of 14.0 km. The high values of H_S are in the right forward quadrant with a maximum H_S of 16 m. This is consistent with earlier studies (Moon *et al.*, 2003), which showed that the wave generation on the typhoon center has an asymmetric distribution in four quadrants.

5.2 Directional wave spectra

Figure 13 shows the daily evolution of directional wave spectra at L-II. The arrow indicates the wind vector at each moment. Before 1800UTC on 20 November, the winds (7.8 m/s) blow from northeast (45° from the north) showing the dominant winter monsoon. The waves are mostly generated downwind (southwestward direction) with frequencies about 0.1–0.25 Hz (Figs. 13(a)–(e)).

From 1800UTC on 20 November to 1800UTC on 23 November, TY Muifa moved across the SCS with low translation speed (2.9 m/s, see Fig. 3). Waves occur in

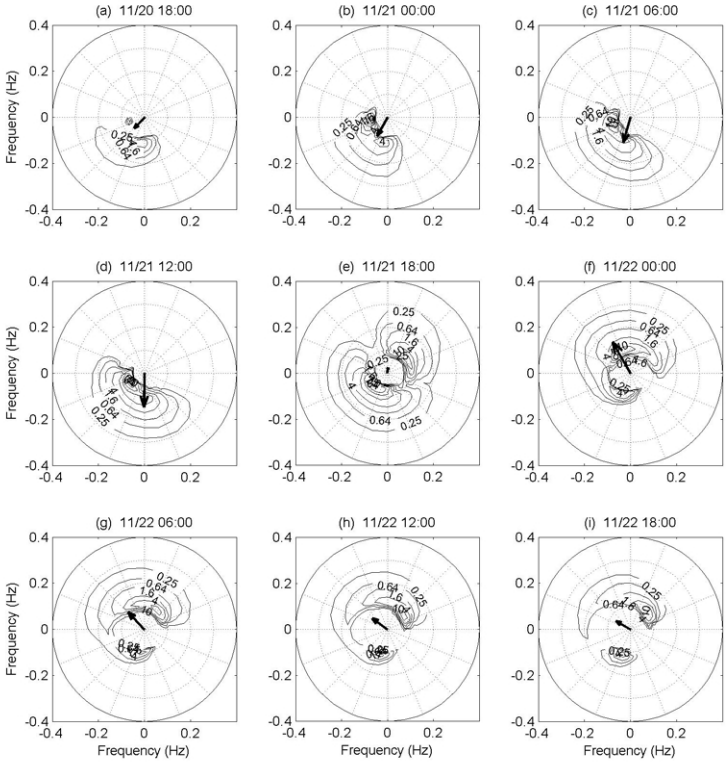

Fig. 14. Six-hour evolution of directional wave spectra with QTCWPM winds on L-II (11.6°N and 114.4°E) from 1800UTC on 20 November to 1800UTC on 21 November. TY Muifa was at this location at 1800UTC on 21 November. Arrow presents QTCWPM wind speed and direction. Wind speed of 40 m/s corresponds to a length of 0.15 Hz.

almost all directions (Figs. 13(f) and (g)) with generation of higher frequency waves up to 0.3 Hz. After the departure of TY Muifa, two evident wave packets remain in the southwestward (90° to 145°) and northeastward (30° to 70°) directions with frequencies around 0.1–0.25 Hz (Figs. 13(h) and (i)).

Variation of the directional wave spectra during TY Muifa's passage at L-II is represented using 6-hr spectral evolution (Fig. 14) from 1800UTC on 20 November to 1800UTC on 22 November. While the winds increase and turn counterclockwise as TY Muifa passes by, the waves are generated along with the turning wind directions. Prior to the typhoon's arrival at L-II, a wide range of waves are generated with monsoon dominated swells in the southwestward direction with frequencies around 0.1–0.3 Hz (Figs. 14(a)–(d)). Upon the typhoon's arrival on 1800UTC on November 21 at L-II, two wave packets are generated in the northeastward and southwestward directions (Fig. 14(e)). These typhoon-generated waves, especially in the opposite direction to monsoon winds (i.e., blowing southwestward), decay rapidly but still exist four days after the typhoon's departure (Fig. 13(i)).

Four points are selected around the TY Muifa's center with the distance of RMW (i.e., R_{max}, see Table 1) to investigate the effect of translation speed on the directional wave spectra: forward (F), backward (B), rightward (R), and leftward (L) (see upper-left panel of Figs. 15 to 18). The typhoon's center is indicated by "C". Four points (F, R, B, L) are marked on the circle with the RMW. The hollow arrow indicates the typhoon's translation velocity vector. The solid arrow is the wind vector at each location. Consistent with the previous study (Moon *et al.*, 2003), the directional wave spectra at the F- and R-points show the generation of high-frequency waves aligning with the wind direction due to resonant effects. The wave spectra at the L- and B-points have more complicated structures.

6. Factors Affecting the Wave Characteristics

Significant wave height and directional wave spectrum are controlled by the winds and topography. The wind forcing (1)–(3) includes the storm track, typhoon transmission speed, storm intensity, and monsoon winds. The significant wave height is influenced by all these wind factors. However, the directional wave spectrum is dependent on the storm track, the resonant effect (or the storm translation speed), and the spatial distribution of winds, which is independent of the storm intensity. Since

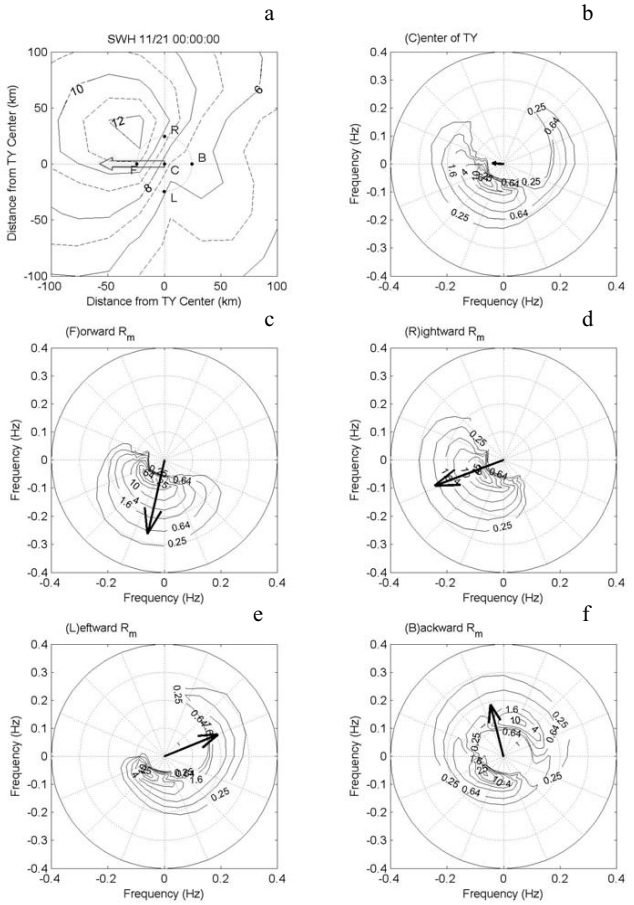

Fig. 15. Wave characteristics at L-I (11.9°N, 117.2°E, 0000UTC on 21 November): (a) horizontal distribution of H_S and directional wave spectra at (b) typhoon center and four-way locations around the TY Muifa center with RMW away (c) forward, (d) backward, (e) rightward, and (f) leftward. Note that the hollow arrow represents the typhoon translation velocity (5.8 m/s) and the solid arrows denote the winds. Wind speed of 40 m/s corresponds to a length of 0.3 Hz.

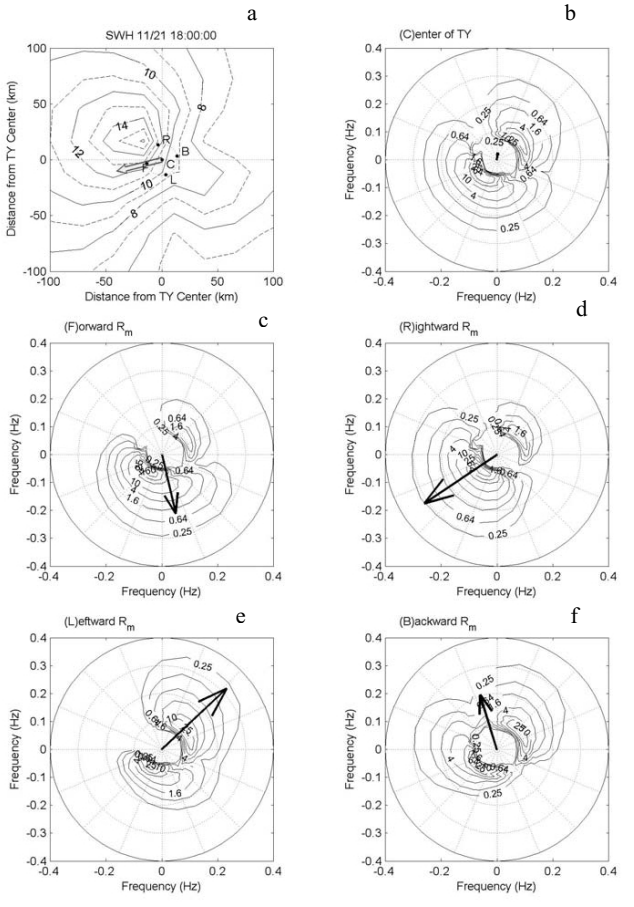

Fig. 16. Wave characteristics at L-II (11.6°N, 114.4°E, 1800UTC on 21 November): (a) horizontal distribution of H_S and directional wave spectra at (b) typhoon center and four-way locations around the TY Muifa center with RMW away (c) forward, (d) backward, (e) rightward, and (f) leftward. Note that the hollow arrow represents the typhoon translation velocity (4.2 m/s) and the solid arrows denote the maximum winds. Wind speed of 40 m/s corresponds to a length of 0.3 Hz.

SCS has deep water and a shallow shelf and is influenced by the steady monsoon winds, the effects of topography and monsoon winds on the wave characteristics are unique in the SCS, and may not be representative of the western North Atlantic.

6.1 Typhoon translation speed

The resonant effect for a rapidly moving typhoon with translation speed is comparable to the group speed of dominant waves (around 10 m/s). The waves to the right of the typhoon track are exposed to prolonged forcing from the wind; that is, they become "trapped" within the typhoon. The trapped waves become dominating swell, propagating in the direction of the track and may overwhelm locally generated wind waves at later times. However, TY Muifa was moving slowly most of time across the SCS with translation speed of 2.9 to 5.8 m/s from L-I to L-IV. For this slowly moving TY Muifa, the translation speed was too low to generate a dominant swell by the resonant effect. The dominant swell direction is mostly determined by the distance from RMW. Since the four positions around the typhoon are relative to the geographical direction, the angles of local wind to environmental wind change. The translation speed of TY Muifa at the four locations (L-I to L-IV) is much lower than the group velocity (10 m/s) of high waves (see Fig. 3(a)).

6.2 Wind direction

At the four points surrounding the typhoon center

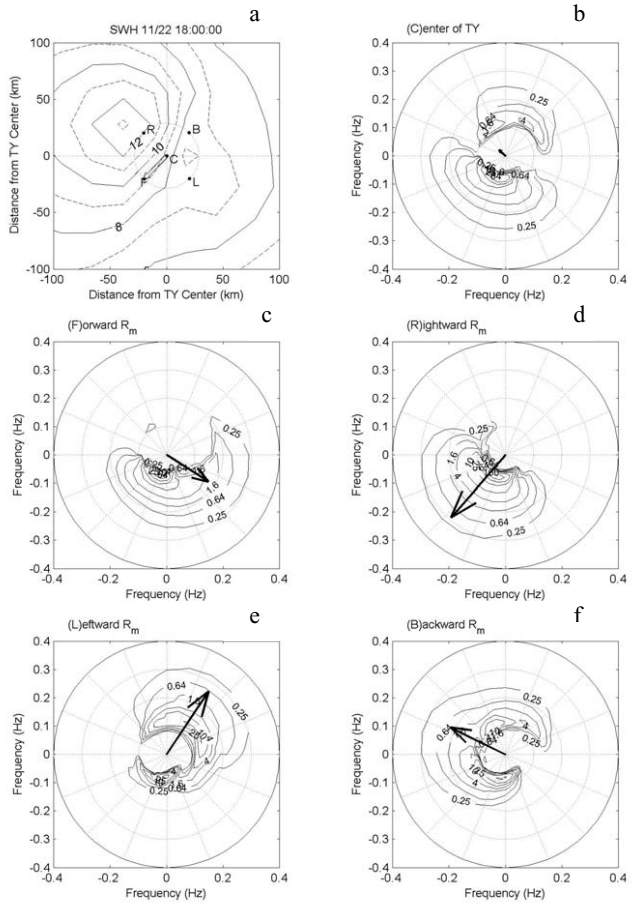

Fig. 17. Wave characteristics at L-III (10.5°N, 112.1°E, 1800UTC on 22 November): (a) horizontal distribution of H_S and directional wave spectra at (b) typhoon center and four-way locations around the TY Muifa center with RMW away (c) forward, (d) backward, (e) rightward, and (f) leftward. Note that the hollow arrow represents the typhoon translation velocity (2.9 m/s) and the solid arrows denote the maximum winds. Wind speed of 40 m/s corresponds to a length of 0.3 Hz.

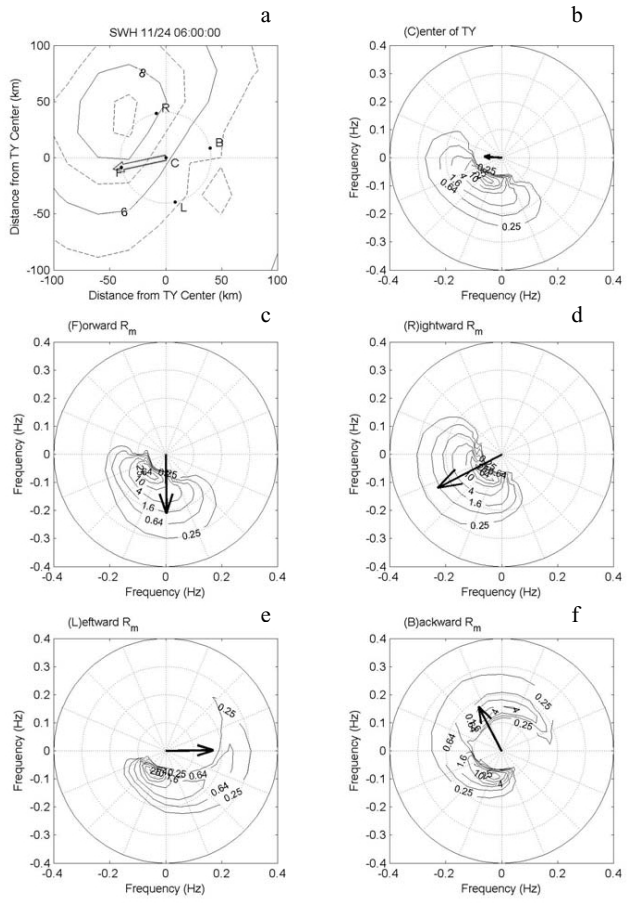

Fig. 18. Wave characteristics at L-IV (8.8°N, 108.8°E, 0600UTC on 24 November): (a) horizontal distribution of H_S and directional wave spectra at (b) typhoon center and four-way locations around the TY Muifa center with RMW away (c) forward, (d) backward, (e) rightward, and (f) leftward. Note that the hollow arrow represents the typhoon translation velocity (4.8 m/s) and the solid arrows denote the maximum winds. Wind speed of 40 m/s corresponds to a length of 0.3 Hz.

(F, B, L, R), the directional wave spectrum is more symmetrical around the wind vector when the wind direction is more likely aligned to the typhoon movement (i.e., positive inner product of wind vector ($\mathbf{V}$) and typhoon translation velocity ($\mathbf{V}_T$)),

$$\mathbf{V} \bullet \mathbf{V}_T > 0. \tag{10}$$

Such a feature does not depend on typhoon intensity and translation speed. For example, the typhoon has the same intensity (33 m/s) at L-1 and L-III, but has higher translation speed at L-1 (around 5.8 m/s) than at L-III (around 2.9 m/s) (Fig. 3). The directional wave spectrum is quite symmetric for L-I and L-III when condition (10) is satisfied (see Figs. 15(c), 15(d), 15(f), 17(c), 17(d), and 17(f)). On the other hand, when the wind direction is not aligned with the typhoon translation velocity (i.e., $\mathbf{V} \bullet \mathbf{V}_T < 0$), the directional wave spectrum is asymmetric around the wind vector, no matter how high the typhoon intensity and translation speed are (see Figs. 15(e), 16(e), 17(e), and 18(e)). Such an effect of wind direction on directional wave spectrum is not evident at the typhoon center since the winds are weak there.

6.3 Typhoon intensity

The typhoon intensity (i.e., typhoon low pressure, p) is closely related to the maximum significant wave height ($H_{S\max}$). Hsu (2006) uses the following linear rela-

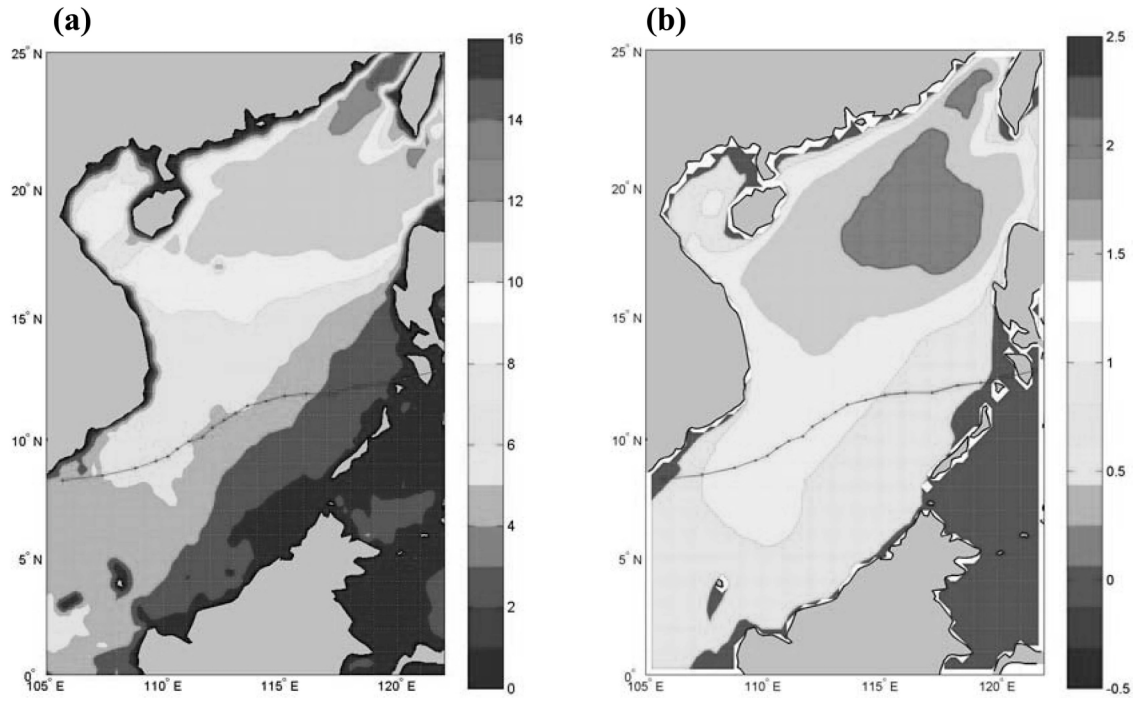

Fig. 19. Differences between two cases (with monsoon winds minus without monsoon winds) in: (a) maximum wind speed, and (b) maximum H_S.

tionship

$$H_{S\max} = 0.2(1013 - p), \tag{11}$$

to predict $H_{S\max}$ of a hurricane from its intensity. As center of TY Muifa moves from L-II to L-IV, the intensity weakens from 954 μPa to 987 μPa. The maximum H_S is 6–7 m larger and is located closer to the typhoon center at L-II than at L-IV (Fig. 12), which is consistent with the empirical formula (11).

6.4 Topography

Wave velocity-bottom topographic interaction is strong in shallow water and weak in deep water. Such interaction results in modulations in the (wave) surface velocity, which in turns causes variations in the surface wave spectrum. Complicated topography gives the SCS a special role in determining the topographic effect. Locations of L-II and L-IV are chosen to identify the effect of topography on the directional spectrum. This is because the typhoon translation speeds are similar at L-II (4.2 m/s) and L-IV (4.8 m/s), the typhoon intensity mainly influences the maximum H_S, and the water depth is around 2600 m at L-II (deep water) and 100 m at L-IV (continental shelf). Between L-II and L-IV the simulated H_S patterns are similar for the typhoon center and six-hour before typhoon arrival.

Among the four points around the typhoon center, the directional wave spectra are very different at F- and R-points but less different at other points due to stronger winds in these two points during typhoon passage. At the F- and R-points, strong waves are generated in all directions over deep water (L-II, Fig. 16), but only in the downwind direction over shallow water (L-IV, Fig. 18). At the other points (typhoon center, L-, and B-points), strong waves are generated in all directions (Figs. 16 and 18), no matter deep or shallow the water. This indicates that the topographic modulation enhances when wind increases. Such a feature has not been previously discussed in tropical cyclones moving over open oceans.

6.5 Monsoon winds

To investigate the monsoon-wind effect on the SCS wave characteristics during TY Muifa's passage from 17 to 25 November, we ran WW3 without the monsoon winds (i.e., $\mathbf{V}_{en} = 0$ in (2)) and compared to that with the monsoon winds ($\mathbf{V}_{en} \neq 0$). The difference in the SCS wave characteristics between the two (with the monsoon-winds ($\mathbf{V}_{en} \neq 0$) minus without the monsoon-winds ($\mathbf{V}_{en} = 0$)) shows the monsoon-wind effect. Such differences in the maximum wind speed and H_S display relatively small values near the typhoon track and relatively large values away from it, especially in the deep water area of the north SCS, where high waves were produced further from the

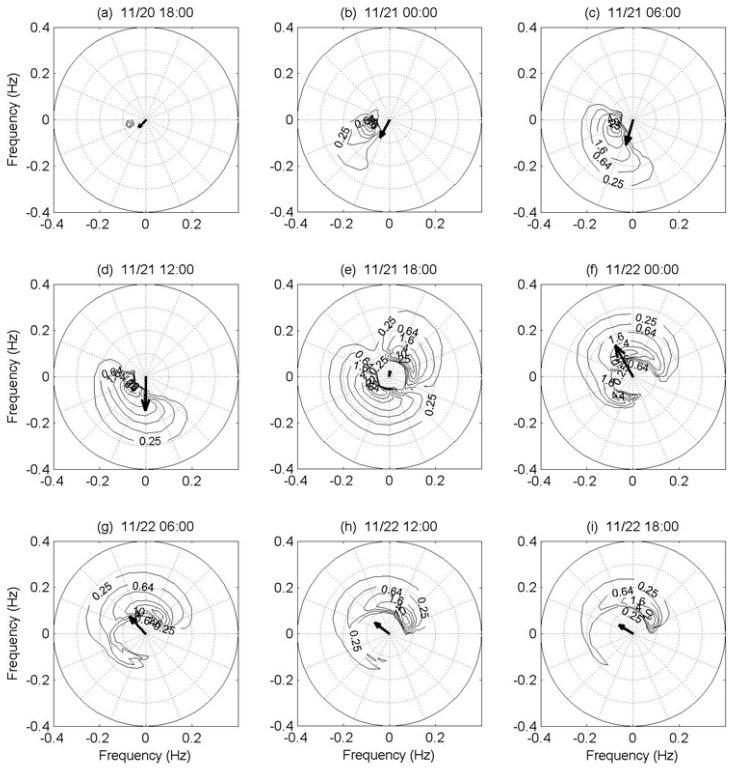

Fig. 20. As Fig. 15 except without monsoon winds ($\mathbf{V}_{en} = 0$).

coast (Fig. 19). This indicates a fetch-limited case forced by the steady monsoon winds.

To investigate the difference in the directional wave spectra between using QTCWPM winds with $\mathbf{V}_{en} = 0$ during TY Muifa's passage, a 6-hr spectral evolution at L-II is presented (Fig. 20) from 1800UTC 20 November to 1800UTC 22 November. Comparing Fig. 20 to Fig. 14, it is found that the two directional wave spectra are almost the same from 0600UTC 21 November to 0600UTC 22 November (24-hr duration of TY Muifa over L-II), but quite different for other time periods. Before TY Muifa's arrival at L-II (1800UTC 21 November), there is a high wave energy center in the southwestward direction with the monsoon winds (Fig. 14(a)) but none without the monsoon winds (Fig. 20(a)). One day after the typhoon's departure from L-II (1800UTC 22 November), the typhoon-generated waves in the southwestward direction dispersed, and the swell energy appeared once again (Figs. 13(a) and (i)). This suggests that the monsoon-generated swell does not decay and remains throughout the typhoon period.

7. Conclusions

This study has investigated the South China Sea wave characteristics using WW3 with winter typhoon forcing. The model was forced by a high resolution wind field, obtained from the QuikSCAT data combined with the tropical cyclone wind profile model. The WW3 model was evaluated using the TOPEX/Poseidon altimetry observation during the period of Typhoon Muifa (2004). Along the typhoon's translation track, the core of the maximum significant wave height (H_S) was asymmetric with higher H_S and wider core on the right side than the left. The maximum H_S was about 16 m, located at the typhoon's minimum lowest pressure center. At a single position, the maximum H_S was always in the right-front quadrant of the typhoon center. Consistent with the previous study (Moon *et al*., 2003), the directional wave spectra in the forward and rightward locations show the generation of high-frequency waves aligning with the wind direction due to resonant effects.

The typhoon's translation speed has different effects on the directional wave spectrum in different directions. An increase of the translation speed enhances the symmetry of the directional wave spectrum around the wind vector in the forward direction, and asymmetry of the directional wave spectrum around the wind vector in the other directions especially at the typhoon center, rightward and backward directions. At the typhoon center, high wave energy centers occur in both forward and backward

directions for the slower translation speed (2.9 m/s) but not for the more rapid translation speed (5.8 m/s).

Typhoon intensity changes the magnitude of the H_S field, but not the horizontal structure, especially the directional wave spectrum. The maximum H_S is at least 6 m larger and is located closer to the typhoon's center for the maximum wind of 46 m/s (at L-II) compared to 26 m/s (at L-IV).

Bottom topography modulates the (wave) surface velocity and causes variations in the surface wave spectrum. This modulation enhances when the wind strengthens. During the typhoon's passage, bottom topography does not affect the simulated H_S patterns for the typhoon's center and six hours before the typhoon's arrival, but it does affect the simulated H_S patterns six hours after the typhoon's departure. Bottom topography strongly affects the directional wave spectrum at the forward and rightward points (stronger winds) but weakly at the other points (weaker winds). At the forward and rightward points, strong waves are generated in all directions over deep water (L-II), but only in the downwind direction over shallow water (L-IV). At the other points (typhoon center, leftward, and backward), strong waves are generated in all the directions no matter deep or shallow the water.

Monsoon winds weakly affect the H_S field near the typhoon's track and strongly away from the track, especially in the deep water area of the north SCS. The steady monsoon winds produce high waves further from the coast (fetch-limited case).

Monsoon winds do not affect the directional wave spectrum within a 24-hr period around the typhoon's passage but they do affect the directional wave spectrum for other periods. One day before TY Muifa's arrival, there is high wave energy center in the southwestward direction with the monsoon winds but none without the monsoon winds. One day after the typhoon's departure, the typhoon-generated waves in the southwestward direction dispersed, and the swell energy appeared once again. The monsoon-generated swell does not decay and remain through the typhoon period.

The simulated wave fields show the effects of typhoon translation speed, intensity, topography, and monsoon winds. However, it is noted that these effects apply only to this case. Further investigation is needed, especially observations of the wave characteristics during a typhoon's passage.

Acknowledgements

The authors wish to thank Dr. Tolman at the National Weather Service for providing the WW3, the NOAA-CIRES Climate Diagnostics Center for providing NCEP Reanalysis data, and NASA/JPL for providing TOPEX/POSEIDON data; they also thank three anonymous reviewers for invaluable comments. This work was jointly funded by the Naval Oceanographic Office, and the Naval Postgraduate School.

References

Barber, N. F. and F. Ursell (1948): The generation and propagation of ocean waves and swell. Part-I. Wave periods and velocities. *Phil. Trans. Roy. Soc. London, Ser. A., Math. Phys. Sci.*, **240**, 527–560.

Booij, N. and L. H. Holthuijsen (1987): Propagation of ocean waves in discrete spectral wave models. *J. Comp. Phys.*, **68**, 307–326.

Bretherton, F. P. and J. R. Garrett (1968): Wave trains in inhomogeneous moving media. *Proc. R. Soc. Lond. (A)*, **302**, 529–554.

Carr, L. E., III and R. L. Elsberry (1997): Models of tropical cyclone wind distribution and beta-effect propagation for application to tropical cyclone track forecasting. *Mon. Wea. Rev.*, **125**, 3190–3209.

Chu, P. C. and K. F. Cheng (2007): Effect of wave boundary layer on sea-to-air dimethylsulfide transfer velocity during typhoon passage. *J. Mar. Sys.*, **66**(1–4), 122–129.

Chu, P. C., N. L. Edmons and C. W. Fan (1999): Dynamical mechanisms for the South China Sea seasonal circulation and thermohaline variabilities. *J. Phys. Oceanogr.*, **29**, 2971–2989.

Chu, P. C., C. W. Fan and W. T. Liu (2000a): Determination of sub-surface thermal structure from sea surface temperature. *J. Atmos. Oceanic Technol.*, **17**, 971–979.

Chu, P. C., J. M. Veneziano, C. W. Fan, M. J. Carron and W. T. Liu (2000b): Response of the South China Sea to tropical cyclone Ernie 1996. *J. Geophys. Res.-Oceans*, **105**, 13991–14009.

Chu, P. C., Y. Q. Qi, Y. C. Chen, P. Shi and Q. W. Mao (2004): South China Sea wind-wave characteristics. Part I: Validation of Wavewatch-III using TOPEX/Poseidon data. *J. Atmos. Oceanic Technol.*, **21**, 1718–1733.

Holden, G. J. and L. R. Wyatt (1992): Extraction of sea state in shallow water using HF radar. *IEE Proceedings-F*, **139**(2), 175–181.

Holt, B., A. K. Liu, D. W. Wang, A. Gnanadesikan and H. S. Chen (1998): Tracking storm-generated waves in the northeast Pacific Ocean with ERS-1 synthetic aperture radar imagery and buoys. *J. Geophys. Res.-Oceans*, **103**, 7917–7929.

Hsu, S. A. (2006): Nowcasting the significant wave height during a hurricane. *Mariners Wea. Log*, **50**(3), 2006 (from http://www.vos.noaa.gov/MWL/dec_6/waveheight.shtml).

Hwang, P. A. and D. W. Wang (2001): Directional distributions and mean square slopes in the equilibrium and saturation ranges of the wave spectrum. *J. Phys. Oceanogr.*, **31**, 1346–1360.

JTWC (2005): 2004 Annual Tropical Cyclone Report [available online at http://www.npmoc.navy.mil/jtwc/atcr/2004atcr/].

Longuet-Higgins, M. S. and R. W. Stewart (1961): The changes in amplitudes of short gravity waves on steady non-uniform currents. *J. Fluid Mech.*, **10**, 529–549.

Moon, I., I. Ginis, T. Hara, H. L. Tolman, C. W. Wright and E. J. Walsh (2003): Numerical simulation of sea surface di-

rectional wave spectra under hurricane wind forcing. *J. Phys. Oceanogr.*, **33**, 1680–1706.

Tolman, H. L. (1999): User manual and system documentation of WAVEWATCH-III version 1.18. Vol. NOAA/NCEP Technical Note 166, US Department of Commerce, 110 pp.

Tolman, H. L. and D. Chalikov (1996): Source terms in a third-generation wind wave model. *J. Phys. Oceanogr.*, **26**, 2497–2518.

Tolman, H. L., B. Balasubramaniyan, L. D. Burroughs, D. V. Chalikov, Y. Y. Chao, H. S. Chen and V. M. Gerald (2002): Development and implementation of wind-generated ocean surface wave models at NCEP. *Weather Forecast*, **17**, 311–333.

Tolman, H. L., J.-H. G. M. Alves and Y. Y. Chao (2005): Operational forecasting of wind-generated waves by hurricane Isabel at NCEP. *Weather Forecast*, **20**, 544–557.

Walsh, E. J., D. W. Hancock, III, D. E. Hines, R. N. Swift and J. F. Scott (1989): An observation of the directional wave spectrum evolution from shoreline to fully developed. *J. Phys. Oceanogr.*, **19**, 670–690.

Whitham, G. B. (1965): Nonlinear dispersion waves. *Proc. R. Soc. Lond. (A)*, **283**, 238–261.

Wittmann, P. A. and P. D. Farra (1997): Global, regional and coastal wave prediction. *Marine Tech. J.*, **31**(1), 76–82.

Wright, C. W., E. J. Walsh, D. Vandemark, W. B. Krabill, A. W. Garcia, S. H. Houston, M. D. Powell, P. G. Black and F. D. Marks (2001): Hurricane directional wave spectrum spatial variation in the open ocean. *J. Phys. Oceanogr.*, **31**, 2472–2488.